



Minerva Access is the Institutional Repository of The University of Melbourne

Author/s:

Wei, GY;Hood, AVS;Planavsky, NJ;Li, D;Ling, HF;Tarhan, LG

Title:

Calcium Isotopic Constraints on the Transition From Aragonite Seas to Calcite Seas in the Cambrian

Date:

2022-05-01

Citation:

Wei, G. Y., Hood, A. V. S., Planavsky, N. J., Li, D., Ling, H. F. & Tarhan, L. G. (2022). Calcium Isotopic Constraints on the Transition From Aragonite Seas to Calcite Seas in the Cambrian. *Global Biogeochemical Cycles*, 36 (5), <https://doi.org/10.1029/2021GB007235>.

Persistent Link:

<https://hdl.handle.net/11343/332937>

Calcium isotopic constraints on the transition from aragonite seas to calcite seas in the Cambrian

Guang-Yi Wei^{1,2*}, Ashleigh v. S. Hood^{2,3}, Noah J. Planavsky², Da Li⁴, Hong-Fei Ling¹, Lidya G. Tarhan^{2*}

¹*State Key Laboratory for Mineral Deposits Research, School of Earth Sciences and Engineering, and Frontiers Science Center for Critical Earth Material Cycling, Nanjing University, Nanjing 210023, China*

²*Department of Earth and Planetary Sciences, Yale University, New Haven, CT 06520, USA*

³*School of Earth Sciences, University of Melbourne, Parkville, VIC 3010, Australia*

⁴*College of Marine Science and Engineering, Nanjing Normal University, Nanjing 210023, China*

*Corresponding authors: Guang-Yi Wei (guangyiwei@nju.edu.cn) (ORCID:

<https://orcid.org/0000-0002-0995-8923>); Lidya G. Tarhan (lidya.tarhan@yale.edu) (ORCID:

<https://orcid.org/0000-0002-5878-929X>)

Abstract

The primary mineralogy of marine carbonates has varied over geological time in concert with the secular evolution of global climate and seawater chemistry. Here, we employed a multi-proxy geochemical and petrographic approach, including measuring the Ca isotope ($\delta^{44}\text{Ca}$) and Sr content of Ediacaran–Cambrian carbonates, to provide new insights into the timing of the transition from a “dolomite-aragonite sea” to a “calcite sea” across the Ediacaran–Cambrian transition. We find robust evidence for the persistence of an aragonite sea well into

Cambrian Age 2 (and potentially up through Age 4). However, together with an updated

This is the author manuscript accepted for publication and has undergone full peer review but has not been through the copyediting, typesetting, pagination and proofreading process, which may lead to differences between this version and the [Version of Record](#). Please cite this article as doi: [10.1029/2021GB007235](https://doi.org/10.1029/2021GB007235).

petrographic compilation of abiotic carbonate precipitates (i.e., ooids and cements), these new $\delta^{44}\text{Ca}$ and Sr data provide further evidence that there was a protracted transition from aragonite seas to calcite seas in the Cambrian. We propose that this transition was mediated, in part, by changes in seawater Mg/Ca ratios potentially regulated by the global marine redox state and extents of authigenic clay precipitation.

1. Introduction

Prior to widespread pelagic carbonate production in the Mesozoic (Wilkinson & Algeo, 1989; Martin, 1995; Ridgwell & Zeebe, 2005; Blättler et al., 2012), shallow-marine carbonates constitute the majority of carbonate lithologies preserved in the geological record. These shallow-marine carbonates are commonly used as archives for past global climate and oceanic chemical conditions (e.g., Hardie, 1996; Ridgwell & Zeebe, 2005; Wallace et al., 2017; Cantine et al., 2020). Changes in marine chemistry, global climate and biogeochemical cycling have long been implicated as factors that have mediated shifts in shallow-marine carbonate mineralogy (Hardie, 1996, 2003; Stanley & Hardie, 1998; Holland, 2005; Porter, 2007, 2010). It is now generally accepted that the mineralogy of shallow-marine carbonates has oscillated broadly through the Phanerozoic between “aragonite seas” during which primary carbonate precipitation was dominated by aragonite and high-Mg calcite, and intervals characterized by “calcite seas” during which primary carbonate precipitation was dominated by calcite (Sandberg, 1983; Stanley & Hardie, 1998; Porter, 2010). Phanerozoic variations in shallow-marine carbonate mineralogy and associated transitions in seawater chemistry have traditionally been constrained via the petrographic analysis of ‘biotic’ (skeletal) and ‘abiotic’ carbonates (ooids and cements) (e.g., Sandberg, 1983; Stanley & Hardie, 1998; Porter, 2007,

2010; Zhuravlev & Wood, 2008; Wood et al., 2017; Hood & Wallace, 2018). Petrographic data, including skeletal macrofossils, ooids and marine cements, suggest that the Neoproterozoic Era may have been characterized by “aragonite-dolomite seas”, during which primary shallow-marine carbonates were dominated by aragonite, high-Mg calcite and dolomite (Tucker, 1989; 1992; Hood et al., 2011; Hood & Wallace, 2012, 2018; Wood et al., 2017). Several studies have highlighted that the mineralogy of the carbonate factory in the Cambrian may have been more variable and aragonite deposition may have been more common than traditional envisioned (Zhuravlev & Wood, 2008; Wood et al., 2017; Hood & Wallace, 2018). Well-preserved shallow-marine cements and ooids can be useful petrographic indicators of marine carbonate mineralogy, (e.g., Hood & Wallace, 2018), but successions in which these archives are sufficiently stratigraphically abundant to provide extensive and relatively continuous records of depositional mineralogy in the Neoproterozoic and Cambrian have not been systemically investigated.

Emerging geochemical proxies can provide independent, novel and relatively high-resolution insights regarding marine and early diagenetic variations in shallow-marine carbonate mineralogy (e.g., Higgins et al., 2018; Pruss et al., 2018). For instance, calcium isotope ($\delta^{44}\text{Ca}$) and strontium (Sr) content data, when collected in tandem, represent a powerful tool that can provide constraints on primary carbonate mineralogy, as well as carbonate precipitation rates and early diagenetic process (Veizer, 1983; Gussone et al., 2005; Higgins et al., 2018; Pruss et al., 2018; Wang et al., 2020; Ahm et al., 2021; Busch et al., 2022; Wei et al., 2022). Compared to petrographic observations, geochemical analyses can provide higher-resolution records of primary mineralogy and early diagenetic history from a broader range of

bulk carbonate lithologies, especially for micrites as well as sediments that have undergone early recrystallization and dolomitization and may be less amenable to petrographic identification of original mineralogy. Here, we present a new set of $\delta^{44}\text{Ca}$ and Sr content data from marine carbonates in South China, ranging in age from the terminal Ediacaran through the lower Cambrian (ca. 551–509 Ma). The $\delta^{44}\text{Ca}$ and Sr data generated from these successions are characterized by long-term variability, which we interpret to potentially record changes in primary carbonate mineralogy, precipitation rates and/or modes of early marine diagenesis. We further compare these Ca isotope and Sr concentration data to a new compilation of petrographic data recording the primary carbonate mineralogy of ooids and marine cements spanning the upper Ediacaran to upper Cambrian, building upon data published in previous studies (e.g., Tucker, 1992; Zhuravlev & Wood, 2008; Hood & Wallace, 2018). Together, these expanded petrographic and new geochemical datasets suggest substantial variability in carbonate mineralogy across the Ediacaran–Cambrian and that the transition between aragonite and calcite seas was notably protracted rather than abrupt. A highly variable marine carbonate system appears to have persisted with biogeochemical instability across the Precambrian–Phanerozoic transition. This adds further complexity to the view of a succinct transition between calcite and aragonite seas in the early Cambrian proposed by some previous studies (e.g., Porter, 2010). Further, the broad agreement between petrographic and geochemical indicators of primary carbonate mineralogy highlights the use of the coupled Ca–Sr system as a reliable indicator of primary carbonate mineralogy and early diagenetic processes in deep time, especially for geologic intervals or stratigraphic successions depauperate in skeletal, ooid and marine cement components.

2. Geological background

We collected samples from two Ediacaran–Cambrian shallow marine carbonate-dominated successions in South China (Fig. 1), the Gaojiaxi–Yanjiahe section in the Yangtze Gorges area, Hubei Province, China, which records an intrashelf basin paleoenvironment (subtidal shale-carbonate facies) from the late Ediacaran to the early Cambrian, and the Xiaotan section, NE Yunnan Province, China, which records an inner shelf paleoenvironment (peritidal carbonate-dominated facies) from the late Ediacaran to the Cambrian (Jiang et al., 2011). Previous studies have included systematic characterization of the biostratigraphy and carbon isotope chemostratigraphy of these two sections, and suggest that they can be correlated, at the sub-stage level, with other, broadly contemporaneous successions globally, including in Morocco, Mongolia and Siberia (e.g., Maloof et al., 2010; Jiang et al., 2012; Li et al., 2013; Bowyer et al., 2022).

In the Gaojiaxi–Yanjiahe section, the upper Ediacaran Dengying Formation can be divided into three members described as, from the base to top, the 1) Hamajing Member (approximately 21 m thick): intraclastic and oolitic dolomitic grainstone; 2) Shibantan Member (approximately 50 m thick): dark grey laminated micritic limestone, with cherty laminae in the upper part; and 3) Baimatuo Member (approximately 40 m thick): micritic and finely crystalline dolostone. Overlying the Dengying Formation is the Yanjiahe Formation, which spans the Ediacaran–Cambrian boundary (Jiang et al., 2012). The Yanjiahe Formation can be divided into two shallowing-upward sub-cycles. The lower sub-cycle (approximately 29 m thick) consists of dark grey laminated dolostone with cherty dolostone, siliceous layers and black shale, and dolostone with cherty and phosphatic clasts. The upper sub-cycle (approximately 25 m thick)

is characterized by a black siliceous lithology interlaminated with black shale and laminated limestone, and limestone with siliceous and phosphatic clasts. The Ediacaran-Cambrian boundary is considered to be recorded at the base of the lower dolostone layer, where the *Anabarites trisulcatus-Protohertzina anabarica* small shelly fossil assemblage zone first occurs in South China (Jiang et al., 2012).

The Xiaotan section comprises, from base to top, the upper Ediacaran Dengying Formation and lower Cambrian Zhujiaping, Shiyantou, Yu'an Shan, Hongjingshao and Wulongqing formations. The Dengying Formation in the Xiaotan section can be divided into three members from the base to top: 1) the Donglongtan Member (approximately 35 m thick), consisting of laminated dolostone; 2) the Jiucheng Member, consisting of poorly outcropping shale; and 3) the Baiyanshao Member (approximately 75 m thick), containing thickly bedded to massive, grey to dark grey, finely crystalline dolostone. The Dengying Formation is overlain by the Cambrian Zhujiaping Formation, comprising three members, from base to top: 1) the Daibu Member (approximately 30 m thick), consisting of interbedded dark, dolomitic chert and pale yellowish siliceous dolostone of thin to intermediate thickness; 2) the Zhongyicun Member (75 m thick), consisting of a thick phosphorite layer interbedded with laminated dolostones, and containing the local Ediacaran-Cambrian boundary as defined in South China by the *Anabarites trisulcatus-Protohertzina anabarica* and *Siphonochites triangularis-Paragloborilus subglobosus* small shelly fossil assemblages (Li & Xiao, 2004); and 3) the Dahai Member (approximately 65 m thick), consisting of pale grey, thickly bedded fossiliferous limestone containing the *Heraultipegma yunnanensis* small shelly fossil assemblage (Li & Xiao, 2004). The Shiyantou Formation, overlying the Zhujiaping Formation, consists of grey to dark grey,

bedded siltstone in its lower part, and dark grey to black shale with a *Sinosachites-Tannuolina* small shelly fossil assemblage in the upper part (Li & Xiao, 2004). The Yu'an-shan Formation, which contains the first regional appearance datum (FAD) of trilobites in its basal strata (local base of Cambrian Stage 3), consists of a lower black shale and upper carbonate-rich siltstone. The Hongjingshao Formation contains dark red, thickly bedded sandstone. The Wulongqing Formation in the Xiaotan section consists of grey, thickly bedded limestone with interbedded yellow silty mudstone, and has been interpreted to have been deposited near the beginning of Cambrian Age 4 (Wei et al., 2018).

3. Analytical methods

Carbonate samples selected for this study consist chiefly of micrite, microsparite, and medium- to finely crystalline dolomite (Fig. 2). Previous geochemical work on these samples, including previously generated uranium isotope data is reported in Wei et al. (2018). Cut blocks of each sample were carefully screened to avoid non-carbonate detrital components and late-stage veins, then ground into 200-mesh powder. Sample powders were leached with 0.1 M hydrochloric acid (HCl) until effervescence ceased in order to extract carbonate-bound major and trace elements without contamination from detrital components. Major and trace element concentrations were measured with a Thermo ElementXR ICP-MS at the Yale Metal Geochemistry Center (YMGC), Yale University. Relative standard deviations were better than 5%, based on repeated analyses of the IAPSO seawater standard. The Ca isotope values of samples were measured using a Thermo Neptune Plus MC-ICP-MS with an ESI Apex-IR desolvating system at the YMG, following the procedures outlined in Wei et al. (2019). The NIST SRM 915a standard was used to calibrate isotopic bias during the measurements with a

sample–standard bracketing method. Measured $^{44}\text{Ca}/^{42}\text{Ca}$ ratios are presented in delta notation, $\delta^{44/42}\text{Ca}$. The long-term external reproducibility of Ca isotope analyses at the YMGC is better than 0.08‰ (2SD) for repeated measurement of IAPSO seawater and NIST SRM 915b standards: $\delta^{44/42}\text{Ca}_{\text{seawater-915a}} = 0.89\text{‰} \pm 0.08\text{‰}$ ($n = 65$, 2SD); $\delta^{44/42}\text{Ca}_{915b-915a} = 0.36\text{‰} \pm 0.07\text{‰}$ ($n = 50$, 2SD), which are consistent with published values (Fantle & Tipper, 2014). All Ca isotope data have been converted to $\delta^{44}\text{Ca}$ ($^{44}\text{Ca}/^{40}\text{Ca}$) notation for comparison with other published data, using a kinetic fractionation law: $\delta^{44}\text{Ca} = 2.05 \times \delta^{44/42}\text{Ca}$, and ultimately reported relative to the IAPSO seawater standard (i.e., $\delta^{44}\text{Ca}_{\text{seawater}} = 0\text{‰}$).

4. Results and discussion

4.1. Geochemical ($\delta^{44}\text{Ca}$ values and Sr content) and petrographic constraints on carbonate mineralogical variations from the late Ediacaran to the early Cambrian

The primary mineralogy and timing of the first appearances of carbonate-biomineralizing metazoan clades (as inferred from petrographic data and the mineralogy of well-preserved fossil specimens and living representatives) are considered to track shifts in marine carbonate mineralogy (Porter, 2010; Wood et al., 2017). However, skeletal fossil material may not be preserved in stratigraphically continuous sections, hampering the reconstruction of continuous records of primary carbonate mineralogy, especially prior to widespread biomineralization. Similarly, other archives commonly used for petrographic determination of original mineralogy (e.g., ooid and marine cement occurrences) may also be stratigraphically discontinuous or obscured by dolomitization or late-stage diagenetic alteration. However, building on these records, higher-resolution geochemical archives from a wider array of carbonate bulk lithologies can provide additional insights into how carbonate mineralogy varied across the

critical interval of the Ediacaran–Cambrian.

Calcium isotopes can provide insights into primary carbonate mineralogy—based on the principle that the isotopic fractionation between primary aragonite and seawater is much larger than that between primary calcite and seawater—despite the potential effects of early diagenetic processes (Blättler & Higgins, 2017; Higgins et al., 2018; Pruss et al., 2018; Ahm et al., 2021) and changes in Ca isotope fractionation factor associated with differences in precipitation rate (Tang et al., 2008; Wang et al., 2020). Large changes in the $\delta^{44}\text{Ca}$ values of bulk carbonates over longer geologic time scales (>1 Myr timescales) have been commonly linked to changes in the carbonate factory (Farkaš et al., 2007; Blättler et al., 2012; Blättler & Higgins, 2017; Pruss et al., 2018; Wei et al., 2019). Marine carbonates are overwhelmingly the main sink of seawater Ca. Therefore, on very long timescales and under steady-state conditions, the average isotopic composition of global carbonates through time should be equivalent to that of the bulk silicate Earth (BSE; $\delta^{44}\text{Ca}_{\text{BSE}} \sim -1\text{‰}$)—i.e., ultimately the source of seawater Ca (e.g., Blättler & Higgins, 2017). One of the major processes that results in carbonate Ca isotopic signatures significantly lower than BSE is aragonite precipitation. In this light, despite variability in $\delta^{44}\text{Ca}$ values and Sr concentrations of global seawater, the combination of notably low $\delta^{44}\text{Ca}$ values (as low as $\sim -1.6\text{‰}$) and high Sr contents (significantly higher than 1000 ppm) of shallow marine (biotic and abiotic) carbonates can be most parsimoniously inferred to reflect a high relative abundance of primary aragonite (Veizer, 1983; Gussone et al., 2005; Blättler & Higgins, 2017; Higgins et al., 2018; Pruss et al., 2018; Ahm et al., 2021). Dolomitization of primary aragonite or neomorphism from an aragonitic precursor to calcite may dramatically increase the $\delta^{44}\text{Ca}$ values and decrease the Sr concentrations of bulk carbonates in platform settings,

where conditions are strongly fluid-buffered (Blättler & Higgins, 2017; Higgins et al., 2018; Ahm et al., 2021). However, these processes will result in higher, rather than lower $\delta^{44}\text{Ca}$ values.

The Ediacaran limestones in this study preserve notably light $\delta^{44}\text{Ca}$ values (as low as -1.66‰) and high Sr concentrations (up to 5801.4 ppm) (Fig. 3), providing clear evidence that carbonates deposited during this interval included substantial primary aragonite. This is consistent with petrographic and geochemical evidence for aragonite from abiotic and skeletal carbonates from the uppermost Ediacaran (Tucker, 1989; Wood et al., 2017; Hood & Wallace, 2018; Pruss et al., 2018). By contrast, Ediacaran dolostones in the studied successions are characterized by relatively high $\delta^{44}\text{Ca}$ values (up to -0.26‰) and extremely low Sr concentrations (as low as 34.1 ppm), which are similar values to those of modern Bahamian diagenetic dolostones (Higgins et al., 2018). Ediacaran dolostones in this study are additionally characterized by relatively high Ba concentrations (Fig. S1), potentially suggesting an aragonitic precursor for these dolostones (cf. Hood et al., 2015). The geochemical signatures of these Ediacaran dolostones are consistent with early dolomitization of primary aragonite under strongly fluid-buffered (e.g., seawater-buffered) conditions (similar to other Neoproterozoic dolostones; e.g., Corsetti et al 2006; Hood & Wallace, 2012, 2018). Early dolomitization of aragonite during this interval is also supported more broadly by observation of common mimetic ooid and cement dolomite replacement textures in Ediacaran carbonate strata (Hood & Wallace, 2018; Hu et al., 2020).

The Fortunian samples included in this study are also mostly dolostones with high $\delta^{44}\text{Ca}$ values (up to -0.51‰), but they show more variable Sr concentrations (14.9–2570.9 ppm) (Fig.

3). Dolostones in this interval with relatively high Sr concentrations mainly come from interbedded dolostones in the Zhongyicun phosphorites, thus their Sr contents may have potentially been affected by local apatite dissolution during dolomitization. Variability in Ca isotope signatures may also be caused by varying carbonate precipitation rates—where more rapid precipitation, at higher carbonate saturation states, will lead to a larger fractionation factor (e.g., Tang et al., 2008; Nielsen et al., 2012; Wang et al., 2020). Under this scenario, variability in Fortunian Ca isotope signatures may not be a signal for extensive diagenetic overprinting.

Cambrian Stage 2 limestone samples, unlike the analyzed Fortunian dolostones, are characterized by notably low $\delta^{44}\text{Ca}$ values (as low as -1.45‰) and high Sr concentrations (up to 4782.6 ppm), strongly indicative of a high relative abundance of primary aragonite, particularly in the Xiaotan section (Fig. 3). Unfortunately, the studied sections do not contain continuous carbonate strata spanning upper Stage 2 through Stage 3. However, Stage 4 limestones show intermediate $\delta^{44}\text{Ca}$ values (\sim -1.06‰) and relatively low Sr concentrations (\sim 350.6 ppm) (Fig. 3), slightly lower than those of modern Bahamian calcites (Higgins et al., 2018), potentially reflecting either neomorphism of primary aragonite, precipitation of primary calcite or a shift in precipitation rates (cf. Wang et al., 2020).

A new compilation of the petrography and inferred primary carbonate mineralogy of upper Ediacaran through upper Cambrian ooids and cements also demonstrates a complex distribution of mineralogical compositions through this interval (Fig. 6C, also see Supplementary Table S1 for detailed descriptions). Upper Ediacaran carbonates in this compilation are commonly characterized by petrographic evidence for a predominantly aragonite or high-Mg calcite

mineralogy, though some low-Mg calcite ooids have been documented (Hood & Wallace, 2018). In contrast, data from our updated petrographic compilation indicate notable variation in primary carbonate mineralogies, including Cambrian instances of primary aragonite, high-Mg calcite (e.g., commonly shown in bi-mineralic ooids) and low-Mg calcite (Fig. 6C). Aragonite fans and cements are more common in the lower Cambrian (James & Klappa, 1983), whereas there appears to have been a gradual increase in the prevalence of low-Mg calcite over time. However, this updated compilation—unlike some previous iterations (e.g., Porter, 2010)—indicates that abiotic aragonite precipitates also occur throughout the Cambrian and may indicate a persistence of aragonite seas rather than short-term oscillations between aragonite and calcite seas as other studies (e.g., Zhuravlev and Wood, 2008; Wood et al., 2017) have proposed.

4.2. Correlated variations in carbonate $\delta^{44}\text{Ca}$ value and Sr concentration: primary mineralogical signal or diagenetic overprinting?

Analyzed Ediacaran and Cambrian limestone samples in this study show stratigraphic variability, with upper Ediacaran to Cambrian Stage 2 limestones characterized by notably low $\delta^{44}\text{Ca}$ values, and Cambrian Stage 4 limestones characterized by relatively higher $\delta^{44}\text{Ca}$ values (Fig. 4). Dolostones throughout the Ediacaran–Cambrian interval are generally marked by relatively variable but commonly high $\delta^{44}\text{Ca}$ values. A variety of processes, both primary (e.g., original precipitation as calcite) and diagenetic (e.g., neomorphism or dolomitization), can result in high $\delta^{44}\text{Ca}$ values. However, significantly low $\delta^{44}\text{Ca}$ values can most parsimoniously be interpreted as recording primary aragonite precipitation.

The low $\delta^{44}\text{Ca}$ isotope values and high Sr contents we observe in limestones from the

studied successions are, when considered in tandem, outside of the range that could be explained by fluid-buffered early diagenesis (regardless of whether that fluid was marine or meteoric) (cf. Ahm et al., 2018). The recurrent prevalence of low $\delta^{44}\text{Ca}$ values and high Sr contents in Ediacaran–Cambrian strata of the Gaojiaxi–Yanjiahe and Xiaotan sections therefore suggests that widespread aragonite precipitation persisted (and aragonite geochemical indicators were preserved) through the late Ediacaran to at least Cambrian Age 2. These observations from South China are also consistent with light Ca isotope signatures and petrographic data from uppermost Ediacaran limestones from the Nama Group of Namibia (-1.60‰ to -1.07‰, average -1.42‰; Pruss et al., 2018; Tostevin et al., 2019). Previous work in the Nama Group has led to suggestions that changes in continental weathering, evaporite deposition or style of dolomitization may have influenced stratigraphic $\delta^{44}\text{Ca}$ variation in these carbonates (Tostevin et al., 2019). However, it is difficult to rule out short-lived changes in carbonate mineralogy (even if background seawater conditions, as reflected by sparser skeletal, cement, ooid and fluid-inclusion records, predominantly favored aragonite or dolomite precipitation through the broader interval of the late Ediacaran). Alternatively, varying fractionation factors associated with carbonate precipitation (tied to locally variable rates of precipitation) could have also played a role in the development and preservation of these geochemical signatures.

Geochemical data from South China therefore suggest that marine dolomite-aragonite precipitation was prevalent during the late Ediacaran and subsequently transitioned to predominantly aragonite precipitation in the early Cambrian (Fig. 4)—prior to the eventual emergence of more widespread calcite precipitation later in the Cambrian—likely reflecting

gradual decreases in the amount of early marine dolomite precipitation. This is reinforced by petrographic evidence indicating that, on a global scale, upper Ediacaran and lower Cambrian ooids and marine cements commonly (though not exclusively) indicate an aragonitic primary mineralogy (Fig. 6, see Supplementary Table S1 for data compilation), consistent with previous constraints on carbonate mineralogical transitions in this interval (e.g., Zhuravlev & Wood, 2008; Wood et al., 2017; Hood & Wallace, 2018). Early diagenetic processes, particularly dolomitization or neomorphism, can significantly alter $\delta^{44}\text{Ca}$ values as well as Sr concentrations of shallow-marine carbonates, as is observed along the modern Bahamian carbonate platform (Ahm et al., 2018; Higgins et al., 2018). The co-variation of multiple geochemical indices in marine carbonates can be linked to changes in the extent (e.g., degree of alteration of the original sediment) and style (fluid-buffered vs. sediment-buffered) of diagenetic processes (Higgins et al., 2018). As one means of exploring the observed $\delta^{44}\text{Ca}$ variability in the South China carbonates, we employed a recently developed early diagenetic model (modified after Ahm et al., 2018) to estimate impacts of extent/style of diagenesis (e.g., along a gradient of fluid-buffered to rock-buffered diagenesis) on carbonate $\delta^{44}\text{Ca}$, Mg/Ca and Sr values of different stratigraphic units in this study. As the rates of recrystallization and/or neomorphism for shallow carbonate platforms are potentially much higher than those of deep-sea carbonates (e.g., Ahm et al., 2018; Higgins et al., 2018), it is possible that early diagenetic processes may have varied between depositional facies and formations (Ahm et al., 2021; Busch et al., 2022).

Using this modeling approach, with parameters selected to represent a range of potential scenarios for Ediacaran–Cambrian shallow marine carbonate successions (see Supplementary materials for details), we were able to reproduce a number of the salient features of the

stratigraphic trends observed in the South China Ediacaran–Cambrian successions. Four main processes during early diagenesis of marine carbonates have been modeled, including dolomitization of primary aragonite (solid lines in Fig. 5B) or primary calcite (solid lines in Fig. 5C), neomorphism from primary aragonite to calcite (dashed lines in Fig. 5B), and recrystallization of primary calcite (dashed lines in Fig. 5C) (see Fig. S2 for carbonate alteration trajectories). The final model results indicate that coherent covariations between $\delta^{44}\text{Ca}$, Mg/Ca and Sr values in each stratigraphic unit could have been reasonably driven by a combination of changes in extent and type of diagenetic process (Fig. 5), assuming that either aragonite or calcite was a primary or precursor mineral (Fig. 5B and C). We further compare the diagenetic endmember of our modeled data (dashed lines in Fig. 5C) to rate-dependent $\delta^{44}\text{Ca}$ and Sr covariations in primary calcites corresponding to varying seawater Ca isotope compositions (solid purple lines in Fig. 5C) (Tang et al., 2008; Wang et al., 2020 and references therein).

Despite high variabilities in $\delta^{44}\text{Ca}$ values and Sr contents, negative correlations are overall observed for these values in all studied carbonates (Fig. 5). This suggests that a combination of primary mineralogy, precipitation rate and/or early diagenetic processes could theoretically shape the geochemical signatures of these upper Ediacaran–lower Cambrian carbonates (cf. Ahm et al., 2018; Higgins et al., 2018; Wang et al., 2020). However, the persistence of notably low $\delta^{44}\text{Ca}$ values and high Sr contents in the limestones of the upper Ediacaran Shibantan Member and the Cambrian Stage 2 Dahai Member most parsimoniously reflect primary aragonite precipitation and limited alteration via early diagenetic pathways (Fig. 5B). Upper Ediacaran and lower Cambrian dolostones in these successions exhibit co-varying relationships between $\delta^{44}\text{Ca}$ and both Mg/Ca ratios and Sr concentrations over a range of parameter space,

indicating that these features in the analyzed dolostones could feasibly result from moderately to highly fluid-buffered conditions during the dolomitization of an aragonitic precursor (Fig. 5B) or, alternatively, substantial variation in precipitation rate. Near-complete dolomitization in most samples under these conditions (Fig. 5B) may have resulted in dolostone compositions reflecting seawater chemistry (cf. Crockford et al., 2020).

This model can also be more broadly applied to other regions and datasets, such as to previously published $\delta^{44}\text{Ca}$ data generated from correlative upper Ediacaran strata in Namibia (Tostevin et al., 2019). In both successions—the Shibantan and Dahai members of South China (this study) and the Nama Group of Namibia (Tostevin et al., 2019)—limestones are consistently characterized by low $\delta^{44}\text{Ca}$ values and high Sr contents, providing robust evidence for deposition of marine aragonitic precursors through substantial portions of these successions. Changes in carbonate diagenetic regimes may have been related to different water depths of the depositional units. As seen in modern Bahamian carbonates (Higgins et al., 2018), and as recently proposed for other carbonates inferred to have been deposited in the late Neoproterozoic (Hoffman and Lamothe, 2019; Busch et al., 2022), carbonate sediments deposited in deeper (i.e., subtidal) settings may be more likely to experience sediment-buffered diagenesis and therefore document primary geochemical signatures. The deposition of limestones in the Shibantan and Dahai members coincides with transgressive system tracts and represent deeper marine (subtidal) depositional settings relative to dolostone intervals (interpreted to record peritidal settings) in these successions (Jiang et al., 2011; Li et al., 2013). These paleoenvironmental differences—and associated differences in preservation potential, with a greater potential for sediment-buffered diagenesis in more subtidal settings—may

provide some explanation for why the Shibantan Member and intervals of the Dahai Member are characterized by the most prominent (and diagnostic) indicators of predominantly aragonitic deposition. Observation of co-varying $\delta^{44}\text{Ca}$ values and Sr contents in the Dahai Member (Fig. 6B), may reflect either changes in diagenetic regimes (i.e., variation between more sediment-buffered and more fluid-buffered conditions) or, alternatively, varying proportions of primary aragonite and calcite. Importantly, either mechanism supports our interpretation that the Dahai Member records prominent contributions from primary aragonite sediments, and thus that substantial aragonite precipitation persisted into Cambrian Age 2.

Cambrian Stage 4 limestones of the Wulongqing Formation from South China (this study) have intermediate $\delta^{44}\text{Ca}$ values and Sr contents that are consistent with either primary calcite precipitation (followed by crystal coarsening) or neomorphism from aragonite to calcite. Although a neomorphism explanation for the geochemical signatures of the studied Cambrian Stage 4 limestones (tan triangles in Fig. 5B and C) may not be a unique solution, modeling $\delta^{44}\text{Ca}$ values and Sr trends suggest that neomorphism of an originally aragonitic precursor (Fig. 5B) is more likely than a primary calcite origin or precipitation rate control for Ca isotope variations in these limestones (Fig. 5C). In summary, although dolomitization or neomorphism may overprint the geochemical composition of these and other, contemporaneously deposited units to varying extents, the $\delta^{44}\text{Ca}$ values and Sr contents of these strata can nonetheless, particularly in limestones, be used to determine primary carbonate mineralogical signatures. The coupled Ca isotope and Sr records we have generated from the Ediacaran–Cambrian succession of South China suggest that, as previously proposed (Hood et al., 2011; Wood et al., 2017; Hood and Wallace, 2018), a dolomite-aragonite sea characterized the late Neoproterozoic

oceans. An interval dominated by primary aragonite precipitation subsequently persisted across the Ediacaran-Cambrian boundary and through at least Cambrian Age 2 and potentially as late as Cambrian Age 4.

The preservation of primary geochemical signatures and the updated compilation of data from abiotic marine precipitates provided by this study provide evidence for the persistence of an aragonite sea through the early Cambrian, with additional evidence for aragonite precipitation continuing throughout the Cambrian. There have, historically, been a wide range of proposals, based on different proxies, regarding the timing of the change between calcite and aragonite seas in the Cambrian (e.g., estimates have spanned the early to late Cambrian; Sandberg, 1983; James & Klappa, 1983; Wilkinson et al., 1985; Hardie, 1996; Zhuravlev and Wood, 2008; Reis, 2010; Porter, 2007, 2010; Neilson et al., 2016; Wood et al., 2017), as well as disagreement regarding whether these changes were persistent or, alternatively, ephemeral and characterized by distinct transitions (cf. Zhuravlev and Wood, 2008; Wood et al., 2017). Although additional $\delta^{44}\text{Ca}$ data from Stage 2–3 carbonates will, we hope, in the future help to refine our understanding of the Cambrian evolution of the carbonate factory, overall, the combination of evidence from petrographic observations and new geochemical data from non-skeletal carbonates presented in this study suggests a more nuanced and protracted transition in the carbonate system across the Precambrian-Cambrian boundary and through the Cambrian. These data also highlight that both aragonite and calcite precipitation may have been common from the middle to late Cambrian (Fig. 6). The proposed duration of the Ediacaran and Cambrian aragonite sea is similar to but perhaps more temporally extensive than previous studies of skeletal carbonates, which recognized a transitional period or transient changes in

seawater major ion composition across this interval (James & Klappa, 1983; Zhuravlev & Wood, 2008; Porter, 2010; Reis, 2010; Neilson et al., 2016). Intriguingly, skeletal carbonate records suggest that members of several calcite-biomineralizing clades (e.g., calcareous brachiopods and archaeocyaths) may have emerged during Cambrian Age 2—i.e., during the same interval in which we observe geochemical and petrographic evidence from non-skeletal carbonates for continued deposition of primary aragonite (Porter, 2010). This variability in carbonate mineralogy could potentially reflect high-frequency oscillations between predominant carbonate mineralogies. Alternatively, this may indicate that additional and spatially variable environmental factors, rather than seawater Mg/Ca ratios alone, such as local differences in temperature or in sulfate or phosphate levels, and species-specific vital effects—all of which can strongly but variably impact aragonite and calcite saturation states (e.g., Burton & Walter, 1987, 1990; Bots et al., 2011)—operated as second-order drivers of local carbonate mineralogy.

4.3 Potential factors controlling Cambrian carbonate mineralogical transitions

Transitions between aragonite and calcite seas have historically been linked to secular changes in seawater chemistry (e.g., Mg/Ca ratio, pH), ocean redox state (e.g., dissolved oxygen, iron and sulfate concentrations) and other surface environmental conditions (e.g., climate, $p\text{CO}_2$, extent of continental weathering) (e.g., Sandberg, 1983; Hardie, 1996, 2003; Stanley & Hardie, 1998; Reis, 2010; Wood et al., 2017; Hood & Wallace, 2018). The previously proposed transition from a predominantly aragonite sea to a calcite sea across the Precambrian-Cambrian boundary has also been considered to be broadly coincident with decreased marine Mg/Ca ratios and widespread marine oxygenation (Wood et al., 2017; Hood & Wallace, 2018; Wood, 2018). Rapid decreases in seawater Mg/Ca ratios, driven by enhanced seafloor spreading

and continental weathering, have been proposed to mark the Precambrian-Cambrian transition (Hardie, 1996; Wood et al., 2017). However, early Cambrian changes in marine Mg/Ca ratios are difficult to explain with varying seafloor spreading rates. Foremost, a pronounced increase in seafloor spreading, resulting in increased Mg removal from seawater, would also have decreased global ocean $^{87}\text{Sr}/^{86}\text{Sr}$, which is opposite to the observed trend and the presence of anomalously high seawater $^{87}\text{Sr}/^{86}\text{Sr}$ values in Cambrian strata (McArthur et al., 2012). Enhanced continental weathering has also been proposed to have decreased global seawater Mg/Ca ratios in the late Neoproterozoic to early Cambrian, due to an inferred substantial input of Ca into seawater linked to Great Unconformity-associated weathering (Peters & Gaines, 2012; Wood et al., 2017; Tostevin et al., 2019). Increases in marine oxygen and sulfate levels, as well as greenhouse conditions and high sea level have also been invoked as potential drivers for a hypothesized early Cambrian transition to a calcite sea (Sandberg, 1983; Stanley & Hardie, 1998; Kump, 2008; Reis, 2010).

Geochemical and petrographic evidence from this study supports a protracted transition in marine carbonate mineralogy from the late Ediacaran through the Cambrian, with a high degree of variability, including precipitation of primary aragonite and calcite (as well as dolomite), rather than an abrupt change from aragonite to calcite seas in the Cambrian. These observations of evolving primary mineralogy mirror our emerging understanding of the gradual nature of changes in the extent and style (e.g., environmentally mediated versus enzymatically controlled) of biomineralization across this interval (Wood, 2018; Wood et al., 2019). Based on the geochemical and petrographic data from non-skeletal carbonates presented in this study, the environmental factors that regulate this carbonate mineralogical transition in the Cambrian may

merit further consideration. Changes in the extent of dolomite formation, oceanic crust alteration and marine authigenic clay formation (reverse weathering) are also important levers on seawater chemistry through the regulation of the marine Mg reservoir, for example as has been inferred for the Cenozoic (Holland & Zimmermann, 2000; Higgins & Schrag, 2015; Dunlea et al., 2017). Changes in reverse weathering—linked to shifts in temperature and biological Si uptake (with the diversification of diatoms)—likely played a key role in driving the observed Cenozoic increase in seawater Mg/Ca ratios (Higgins & Schrag, 2015; Dunlea et al., 2017). Prior to the widespread radiation of siliceous organisms (siliceous sponges, radiolarians, diatoms and some higher plants), the Ediacaran and early Cambrian oceans were most likely characterized by high concentrations of dissolved silica (Maliva et al., 2005; Conley et al., 2017; Trower & Fischer, 2019). Therefore, reverse weathering-mediated authigenic clay precipitation in the Ediacaran and early Cambrian oceans was likely much more widespread relative to the modern ocean (cf. Isson & Planavsky, 2018; Trower & Fischer, 2019), and may have played a more critical role in regulating seawater chemistry.

As Mg and ferrous Fe readily substitute for each other in many authigenic clays (e.g., chlorite, glauconite, saponite) (Michalopoulos & Aller, 1995), changes in ocean redox may have been closely linked to extents of removal of seawater Mg via reverse weathering and oceanic crust alteration (Andrews, 1980; Wallmann et al., 2008; Hood et al., 2018; Krissansen-Totton & Catling, 2020). Recent studies have indicated that the Cambrian ocean was likely characterized by highly dynamic redox states and relatively low background dissolved oxygen and sulfate concentrations (e.g., Sperling et al., 2015; Krause et al., 2018; Wood et al., 2019; Wei et al., 2018, 2021a,b). The persistence of ferruginous anoxic ocean waters through the

Neoproterozoic and early Paleozoic (e.g., Sperling et al., 2015; Song et al., 2018) may therefore have inhibited the reverse weathering or oceanic crust alteration pathways of Mg removal, resulting in a substantially lower Mg marine scavenging flux relative to in a fully oxidized ocean (e.g., Hood and Wallace, 2018). Additionally, the early Paleozoic oceans may have also been marked by relatively low sulfate concentrations (e.g., Wei et al., 2021b), facilitating precipitation of aragonite at even lower Mg/Ca levels (cf. Bots et al., 2011). Spatiotemporal dynamics in marine redox state under relatively low global marine baseline oxygen levels may therefore have been linked to the gradual transition in carbonate mineralogy across the Precambrian boundary and through the Cambrian. In particular, a protracted decline in seawater Mg/Ca ratios—ultimately tied to low oceanic oxygen levels (Fig. 6C, D)—may have delayed the transition to a Paleozoic calcite sea and facilitated greater variability in primary carbonate mineralogy in the terminal Neoproterozoic and Cambrian.

5. Conclusions

This study presents new high-resolution geochemical data (Ca isotope, Mg/Ca ratios and Sr content) from upper Ediacaran through lower Cambrian shallow-marine carbonates in South China, as well as a new petrographic database of primary carbonate mineralogy through this interval. Highly variable $\delta^{44}\text{Ca}$ values, Mg/Ca ratios and Sr contents in upper Ediacaran carbonates indicate, in agreement with previous petrographic studies from other localities, that a dolomite–aragonite sea, dominated by primary aragonite deposition or widespread early diagenetic and fluid-buffered marine dolomitization, was characteristic of the late Ediacaran oceans. Cambrian Stage 2 carbonates, in contrast, are marked by notably low $\delta^{44}\text{Ca}$ values, along with low Mg/Ca ratios and high Sr concentrations, and document a persistence of

aragonite sea conditions, which may have also continued into Cambrian Age 4. With this approach, we provide evidence for a protracted transition between aragonite and calcite seas through the Cambrian. These findings highlight the usefulness of the coupled Ca isotope and Sr concentration systems as a reliable proxy for primary carbonate mineralogy in Earth's geologic past, especially for those intervals without continuous records of skeletal material and/or well-preserved abiotic precipitates. The persistence of an aragonite sea in the early Cambrian likely resulted from a protracted decline in seawater Mg/Ca ratios, potentially linked, at least in part, to the persistence of low-oxygen and ferruginous conditions, as well as a high degree of spatial and temporal redox heterogeneity, through this interval. Low baseline global marine oxidant levels (i.e., oceans characterized by low sulfate and high iron concentrations) may have substantially decreased rates of removal of Mg from seawater and thus delayed decreases in seawater Mg/Ca ratios, facilitating primary aragonite precipitation throughout the Cambrian.

Acknowledgements

This study was funded by National Key Research and Development Program of China (2021YFA0718100); Fundamental Research Funds for Central Universities (14380125) and Frontiers Science Center for Critical Earth Material Cycling Fund (DLTD2102); the Strategic Priority Research Program (B) of the CAS (XDB26000000) and the NSFC program (42002002, 41872002). G.-Y.W. acknowledges support from the program A for Outstanding PhD Candidate of NJU. N.J.P. acknowledges support from the Packard Foundation. A.v.S.H. acknowledges support of an ARC DECRA DE190100988. We thank the editors, S. Pruss, and two anonymous reviewers for comments which improved this manuscript.

Data Availability Statement

All data generated in this study can be found in Mendeley Data (DOI: 10.17632/ctpzj9dzh.1), along with additionally compiled geochemical and carbonate petrographic data. Data archiving is in compliance with FAIR data guidelines.

Author contributions

G.-Y.W., A.v.S.H., N.J.P. and L.G.T. designed the study; G.-Y.W., D.L. and H.-F.L. collected the samples and carried out the geochemical experiments; A.v.S.H. and G.-Y.W. collected and analyzed the petrographic data; G.-Y.W. wrote the manuscript with substantial inputs from A.v.S.H., N.J.P., H.-F.L. and L.G.T.; All the authors contributed to the discussion of the data and results.

Competing interests

The authors declare no competing interests.

References

- Andrews, A. J. (1980). Saponite and celadonite in layer 2 basalts, DSDP Leg 37. *Contribution to Mineralogy and Petrology*, 73, 323–340.
- Ahm, A.-S. C., Bjerrum, C. J., Blättler, C. L., Swart, P. K., & Higgins, J. A. (2018). Quantifying early marine diagenesis in shallow-water carbonate sediments. *Geochimica et Cosmochimica Acta*, 236, 140-159.
- Ahm, A.-S. C., Bjerrum, C. J., Hoffman, P. F., Macdonald, F. A., Maloof, A. C., Rose, C. V., Strauss, J. V. & Higgins, J. A., (2021). The Ca and Mg isotope record of the Cryogenian Trezona carbon isotope excursion. *Earth Planet. Sci. Lett.*, 568, 117002.
- Blättler, C. L., Henderson, G. M., & Jenkyns, H. C. (2012). Explaining the Phanerozoic Ca

isotope history of seawater. *Geology*, 40(9), 843-846.

Blättler, C. L., & Higgins, J. A. (2017). Testing Urey's carbonate–silicate cycle using the calcium isotopic composition of sedimentary carbonates. *Earth and Planetary Science Letters*, 479, 241-251.

Bots, P., Benning, L. G., Rickaby, R. E. M., & Shaw, S. (2011). The role of SO₄ in the switch from calcite to aragonite seas, *Geology*, 39(4), 331-334.

Bowyer, F. T., Zhuravlev, A. Y., Wood, R., Shields, G. A., Zhou, Y., Curtis, A., Poulton, S. W., Condon, D. J., Yang, C., & Zhu, M. (2022). Calibrating the temporal and spatial dynamics of the Ediacaran - Cambrian radiation of animals. *Earth-Science Reviews*, 225, 103913.

Burton, E. A., & Walter, L. M. (1987), Relative precipitation rates of aragonite and Mg calcite from seawater: Temperature or carbonate ion control? *Geology*, 15(2), 111-114.

Burton, E. A., & Walter, L. M. (1990), The role of pH in phosphate inhibition of calcite and aragonite precipitation rates in seawater, *Geochimica et Cosmochimica Acta*, 54(3), 797-808.

Busch, J. F., Hodgkin, E. B., Ahm, A.-S. C., Husson, J. M., Macdonald, F. A., Bergmann, K. D., Higgins, J. A., & Strauss, J. V. (2022). Global and local drivers of the Ediacaran Shuram carbon isotope excursion. *Earth and Planetary Science Letters*, 579, 117368.

Cantine, M. D., Knoll, A. H., & Bergmann, K. D. (2020). Carbonates before skeletons: A database approach. *Earth-Science Reviews*, 201, 103065.

Conley, D. J., Frings, P. J., Fontorbe, G., Clymans, W., Stadmark, J., Hendry, K. R., Marron, A. O., & De La Rocha, C. L. (2017). Biosilicification Drives a Decline of Dissolved Si in the Oceans through Geologic Time. *Frontiers in Marine Science*, 4, 397.

- Corsetti, F. A., Kidder, D. L., & Marengo, P. J. (2006). Trends in oolite dolomitization across the Neoproterozoic–Cambrian boundary: A case study from Death Valley, California, *Sedimentary Geology*, *191*(3-4), 135-150.
- Crockford, P. W., Kunzmann, M., Blättler, C. L., Kalderon-Asael, B., Murphy, J. G., Ahm, A.-S., Sharoni, S., Halverson, G. P., Planavsky, N. J., Halevy, I., & Higgins, J. A. (2020). Reconstructing Neoproterozoic seawater chemistry from early diagenetic dolomite. *Geology*, *49*. <https://doi.org/10.1130/G48213.1>.
- Dunlea, A. G., Murray, R. W., Santiago Ramos, D. P., & Higgins, J. A. (2017). Cenozoic global cooling and increased seawater Mg/Ca via reduced reverse weathering. *Nature Communications*, *8*, 844.
- Fantle, M. S., & Tipper, E. T. (2014). Calcium isotopes in the global biogeochemical Ca cycle: Implications for development of a Ca isotope proxy. *Earth-Science Reviews*, *129*, 148-177.
- Gussone, N., Böhm, F., Eisenhauer, A., Dietzel, M., Heuser, A., Teichert, B. M. A., Reitner, J., Wörheide, G., & Dullo, W.-C. (2005). Calcium isotope fractionation in calcite and aragonite. *Geochimica et Cosmochimica Acta*, *69*(18), 4485-4494.
- Farkaš, J., Böhm, F., Wallmann, K., Blenkinsop, J., Eisenhauer, A., van Geldern, R., Munnecke, A., Voigt, S. & Veizer, J. (2007). Calcium isotope record of Phanerozoic oceans: Implications for chemical evolution of seawater and its causative mechanisms. *Geochim. Cosmochim. Acta*, *71*, 5117-5134.
- Hardie, L. A. (1996). Secular variation in seawater chemistry: An explanation for the coupled secular variation in the mineralogies of marine limestone and potash evaporites over the past 600 m.y. *Geology*, *24*, 279-283.

- Hardie, L. A. (2003). Secular variations in Precambrian seawater chemistry and the timing of Precambrian aragonite seas and calcite seas. *Geology*, *31*, 785-788.
- Higgins, J. A., Blättler, C. L., Lundstrom, E. A., Santiago-Ramos, D. P., Akhtar, A. A., Ahm, A. S. C., Bialik, O., Holmden, C., Bradbury, H., Murray, S. T., & Swart, P. K. (2018). Mineralogy, early marine diagenesis, and the chemistry of shallow-water carbonate sediments. *Geochimica et Cosmochimica Acta*, *220*, 512-534.
- Higgins, J. A., & Schrag, D. P. (2015). The Mg isotopic composition of Cenozoic seawater – evidence for a link between Mg-clays, seawater Mg/Ca, and climate. *Earth and Planetary Science Letters*, *416*, 73-81.
- Hoffman, P. F., & Lamothe, K. G., (2019). Seawater-buffered diagenesis, destruction of carbon isotope excursions, and the composition of DIC in Neoproterozoic oceans. *Proceedings of the National Academy of Sciences USA*, *116*(38), 18874-18879.
- Holland, H. D. (2005). Sea level, sediments and the composition of seawater. *American Journal of Science*, *305*, 220-239.
- Holland, H. D., & Zimmermann, H. (2000). The Dolomite Problem Revisited1: *International Geology Review*, *42*(6), 481-490.
- Hood, A.v. S., & Wallace, M. W. (2012). Synsedimentary diagenesis in a Cryogenian reef complex: Ubiquitous marine dolomite precipitation. *Sedimentary Geology*, *255-256*, 56-71.
- Hood, A.v. S., & Wallace, M. W. (2015). Extreme ocean anoxia during the Late Cryogenian recorded in reefal carbonates of Southern Australia. *Precambrian Research*, *261*, 96-111.
- Hood, A.v. S., & Wallace, M. W. (2018). Neoproterozoic marine carbonates and their

paleoceanographic significance. *Global and Planetary Change*, 160, 28-45.

Hood, A.v. S., Wallace, M. W., & Drysdale, R. N. (2011). Neoproterozoic aragonite-dolomite seas? Widespread marine dolomite precipitation in Cryogenian reef complexes. *Geology*, 39, 871-874.

Hu, Y. J., Cai, C. F., Liu, D. W., Pederson, C. L., Jiang, L., Shen, A. J., & Immenhauser, A. (2020). Formation, diagenesis and palaeoenvironmental significance of upper Ediacaran fibrous dolomite cements. *Sedimentology*, 67, 1161-1187.

Isson, T. T., & Planavsky, N. J. (2018). Reverse weathering as a long-term stabilizer of marine pH and planetary climate. *Nature*, 560(7719), 471-475.

James, N. P., & Klappa, C. F. (1983). Petrogenesis of early Cambrian reef limestones, Labrador, Canada. *Journal of Sedimentary Petrology*, 53(4), 1051-1096.

Jiang, G., Shi, X., Zhang, S., Wang, Y., & Xiao, S. (2011). Stratigraphy and paleogeography of the Ediacaran Doushantuo Formation (ca. 635–551Ma) in South China. *Gondwana Research*, 19(4), 831-849.

Jiang, G., Wang, X., Shi, X., Xiao, S., Zhang, S., & Dong, J. (2012). The origin of decoupled carbonate and organic carbon isotope signatures in the early Cambrian (ca. 542–520Ma) Yangtze platform. *Earth and Planetary Science Letters*, 317-318, 96-110.

Krause, A. J., Mills, B. J. W., Zhang, S., Planavsky, N. J., Lenton, T. M., & Poulton, S. W. (2018). Stepwise oxygenation of the Paleozoic atmosphere. *Nature Communications*, 9(1), 4081.

Krissansen-Totton, J., & Catling, D. C. (2020). A coupled carbon-silicon cycle model over Earth history: Reverse weathering as a possible explanation of a warm mid-Proterozoic climate.

Earth and Planetary Science Letters, 537, 116181.

- Kump, L. R. (2008). The role of seafloor hydrothermal systems in the evolution of seawater composition during the Phanerozoic. In: Lowell, R.P. (Ed.), *Magma to Microbe: Modeling Hydrothermal Processes at Ocean Spreading Centers*. Geophysical Monograph Series 178. American Geophysical Union, Washington, pp. 275-283.
- Li, D., Ling, H.-F., Shields-Zhou, G. A., Chen, X., Cremonese, L., Och, L., Thirlwall, M. & Manning, C. J. (2013). Carbon and strontium isotope evolution of seawater across the Ediacaran–Cambrian transition: Evidence from the Xiaotan section, NE Yunnan, South China. *Precambrian Research*, 225, 128-147.
- Li, G., & Xiao, S. (2004). Tannuolina and Micrina (Tannuolinidae) from the Lower Cambrian of eastern Yunnan, South China, and their scleritome reconstruction. *Journal of paleontology*, 78(5): 900-913.
- Maliva, R. G., Knoll, A. H., & Simonson, B. M. (2005). Secular change in the Precambrian silica cycle: Insights from chert petrology. *Geological Society of America Bulletin*, 117(7), 835-845.
- Maloof, A. C., Porter, S. M., Moore, J. L., Dudas, F. O., Bowring, S. A., Higgins, J. A., Fike, D. A., & Eddy, M. P. (2010). The earliest Cambrian record of animals and ocean geochemical change. *Geological Society of America Bulletin*, 122(11-12), 1731-1774.
- Martin, R. E. (1995), Cyclic and secular variation in microfossil biomineralization: clues to the biogeochemical evolution of Phanerozoic oceans. *Global and Planetary Change*, 11(1-2), 1-23.
- McArthur, J. M., Howarth, R. J., & Shields, G. A. (2012). Chapter 7 - strontium isotope

stratigraphy. The Geologic Time Scale. Elsevier, Boston, 127–144.

Michalopoulos, P., & Aller, R. C. (1995). Rapid clay mineral formation in Amazon delta sediments: reverse weathering and oceanic elemental cycles. *Science*, *270*, 614-617.

Neilson, J. E., Brasier, A. T., & North, C.P. (2016). Primary aragonite and high-Mg calcite in the late Cambrian (Furongian). Potential evidence from marine carbonates in Oman. *Terra Nova*, *28*(5), 306-315.

Nielsen, L. C., DePaolo, D. J., & De Yoreo, J. J. (2012). Self-consistent ion-by-ion growth model for kinetic isotopic fractionation during calcite precipitation, *Geochim. Cosmochim. Acta*, *86*, 166-181.

Peters, S. E., & Gaines, R. R. (2012). Formation of the 'Great Unconformity' as a trigger for the Cambrian explosion. *Nature*, *484*(7394), 363-366.

Porter, S. M. (2007). Seawater chemistry and early carbonate biomineralization. *Science*, *316*(5829), 1302.

Porter, S. M. (2010). Calcite and aragonite seas and the de novo acquisition of carbonate skeletons. *Geobiology*, *8*(4), 256-277.

Pruss, S. B., Blättler, C. L., Macdonald, F. A., & Higgins, J. A. (2018). Calcium isotope evidence that the earliest metazoan biomineralizers formed aragonite shells. *Geology*, *46*(9), 763-766.

Ridgwell, A., & Zeebe, R. (2005). The role of the global carbonate cycle in the regulation and evolution of the Earth system. *Earth and Planetary Science Letters*, *234*(3-4), 299-315.

Ries, J. B. (2010). Review: geological and experimental evidence for secular variation in seawater Mg/Ca (calcite-aragonite seas) and its effects on marine biological calcification.

Biogeosciences, 7, 2795-2849.

Sandberg, P. A. (1983). An oscillating trend in Phanerozoic non-skeletal carbonate mineralogy.

Nature, 305(5929), 19-22.

Song, H., et al. (2017). The onset of widespread marine red beds and the evolution of ferruginous oceans, *Nature Communications*, 8(1), 399.

Sperling, E. A., Wolock, C. J., Morgan, A. S., Gill, B. C., Kunzmann, M., Halverson, G.P., Macdonald, F. A., Knoll, A. H., & Johnston, D. T. (2015). Statistical analysis of iron geochemical data suggests limited late Proterozoic oxygenation. *Nature*, 523(7561), 451-4.

Stanley, S. M., & Hardie, L. A. (1998). Secular oscillations in the carbonate mineralogy of reef-building and sediment-producing organisms driven by tectonically forced shifts in seawater chemistry. *Palaeogeography, Palaeoclimatology, Palaeoecology*, 144, 3-19.

Swart, P. K., & Eberli, G. (2005). The nature of the $\delta^{13}\text{C}$ of periplatform sediments: Implications for stratigraphy and the global carbon cycle. *Sedimentary Geology*, 175, 15-129.

Tang, J., Dietzel, M., Böhm, F., Köhler, S.J., & Eisenhauer, A. (2008). $\text{Sr}^{2+}/\text{Ca}^{2+}$ and $^{44}\text{Ca}/^{40}\text{Ca}$ fractionation during inorganic calcite formation: II. Ca isotopes. *Geochimica et Cosmochimica Acta*, 72, 3733-3745.

Tostevin, R., Bradbury, H. J., Shields, G. A., Wood, R. A., Bowyer, F., Penny, A. M., & Turchyn, A. V. (2019). Calcium isotopes as a record of the marine calcium cycle versus carbonate diagenesis during the late Ediacaran. *Chemical Geology*, 529, 119319.

Trower, E. J., & Fischer, W. W. (2019). Precambrian Si isotope mass balance, weathering, and

- the significance of the authigenic clay silica sink. *Sedimentary Geology*, 384, 1-11.
- Tucker, M. E. (1989). Carbon isotopes and Precambrian–Cambrian boundary geology, South Australia: ocean basin formation, seawater chemistry and organic evolution. *Terra Nova*, 1, 573-582.
- Tucker, M. E. (1992). The Precambrian–Cambrian boundary: seawater chemistry, ocean circulation and nutrient supply in metazoan evolution, extinction and biomineralization. *Journal of the Geological Society*, 149, 655-668.
- Veizer, J. (1983). Chemical diagenesis of carbonates: theory and application of trace element technique. In *Stable Isotopes in Sedimentary Geology*, ed. M. A. Arthur, T. F. Anderson, 1. R. Kaplan, J. Veizer, L. S. Land, pp. III- I-100. Tulsa, Okla: Soc. Econ. Paleontol. Mineral.
- Wallace, M. W., Hood, A. vS., Shuster, A., Greig, A., Planavsky, N. J., & Reed, C. P. (2017). Oxygenation history of the Neoproterozoic to early Phanerozoic and the rise of land plants. *Earth and Planetary Science Letters*, 466, 12-19.
- Wallmann, K., Aloisi, G., Haeckel, M., Tishchenko, P., Pavlova, G., Greinert, J., Kutterolf, S., & Eisenhauer, A. (2008). Silicate weathering in anoxic marine sediments, *Geochimica et Cosmochimica Acta*, 72(12), 2895-2918.
- Wilkinson, B. H., & Algeo, T. J. (1989). Sedimentary carbonate record of calcium-magnesium cycling. *American Journal of Science*, 289(10), 1158-1194.
- Wang, J., Jacobson, A. D., Sageman, B. B., & Hurtgen, M. T. (2020). Stable Ca and Sr isotopes support volcanically triggered biocalcification crisis during Oceanic Anoxic Event 1a. *Geology*, 49(5), 515-519.
- Wei, G.-Y., Hood, A.v. S., Chen, X., Li, D., Wei, W., Wen, B., Gong, Z., Yang, T., Zhang, Z.-F.,

- & Ling, H.-F. (2019). Ca and Sr isotope constraints on the formation of the Marinoan cap dolostones. *Earth and Planetary Science Letters*, *511*, 202-212.
- Wei, G.-Y., Planavsky, N. J., Tarhan, L. G., Chen, X., Wei, W., Li, D., & Ling, H.-F. (2018). Marine redox fluctuation as a potential trigger for the Cambrian explosion. *Geology*, *46*(7), 587-590.
- Wei, G.-Y., Planavsky, N. J., He, T., Zhang, F., Stockey, R., Cole, D. B., Lin, Y.-B., & Ling, H.-F. (2021a). Global marine redox evolution from the late Neoproterozoic to the early Paleozoic constrained by the integration of Mo and U isotope records. *Earth-Science Reviews*, *214*, 103506.
- Wei, G.-Y., Ling, H.-F., Shields, G. A., Hohl, S. V., Yang, T., Lin, Y.-B., & Zhang, F. (2021b). Revisiting stepwise ocean oxygenation with authigenic barium enrichments in marine mudrocks. *Geology*, *49*(9), 1059-1063.
- Wei, G.-Y., Wang, J., Planavsky, N. J., Zhao, M., Bolton, E. W., Jiang, L., Asael, D., Wei, W., & Ling, H.-F. (2022). On the origin of Shuram carbon isotope excursion in South China and its implication for Ediacaran atmospheric oxygen levels. *Precambrian Research*, *375*, 106673.
- Wilkinson, B. H., Owen, R. M., & Carroll, A. R. (1985). Submarine Hydrothermal Weathering, Global Eustasy, and Carbonate Polymorphism in Phanerozoic Marine Oolites. *Journal of Sedimentary Research*, *55*(2), 171-183.
- Wood, R. (2018). Exploring the drivers of early biomineralization. *Emerging Topics in Life Sciences*, *2*, 201-212.
- Wood, R., Liu, A. G., Bowyer, F., Wilby, P. R., Dunn, F. S., Kenchington, C. G., Cuthill, J. F.

- H., Mitchell, E. G., & Penny, A. (2019). Integrated records of environmental change and evolution challenge the Cambrian Explosion. *Nature Ecology & Evolution*, 3(4), 528-538.
- Wood, R. A., Zhuravlev, A. Y., Sukhov, S. S., Zhu, M., & Zhao, F. (2017). Demise of Ediacaran dolomitic seas marks widespread biomineralization on the Siberian Platform. *Geology*, 45(1), 27-30.
- Zhu, M., Yang, A., Yuan, J., Li, G., Zhang, J., Zhao, F., Ahn, S.-Y., & Miao, L. (2018). Cambrian integrative stratigraphy and timescale of China. *Science China Earth Sciences*, 62(1), 25-60.
- Zhuravlev, A.Y., & Wood, R. A. (2008). Eve of biomineralization: Controls on skeletal mineralogy. *Geology*, 36(12), 923-926.

Figure captions

Figure 1. Paleogeographic map of South China from the late Ediacaran to the early Cambrian, and lithostratigraphy of the studied Gaojiaxi–Yanjiahe and Xiaotan sections (modified from Wei et al., 2018). SSF 1–4 represent Small Shelly Fossil Assemblage Zones 1–4 in South China (Li & Xiao, 2004; Jiang et al., 2012). Age constraints are derived from a recent review of Chinese biostratigraphy, chemostratigraphy and chronostratigraphy through this interval (Zhu et al., 2018). The space between strata of the Daibu and Zhongyicun members in the Xiaotan section represents a covered interval in this section (i.e., no sampling in the space).

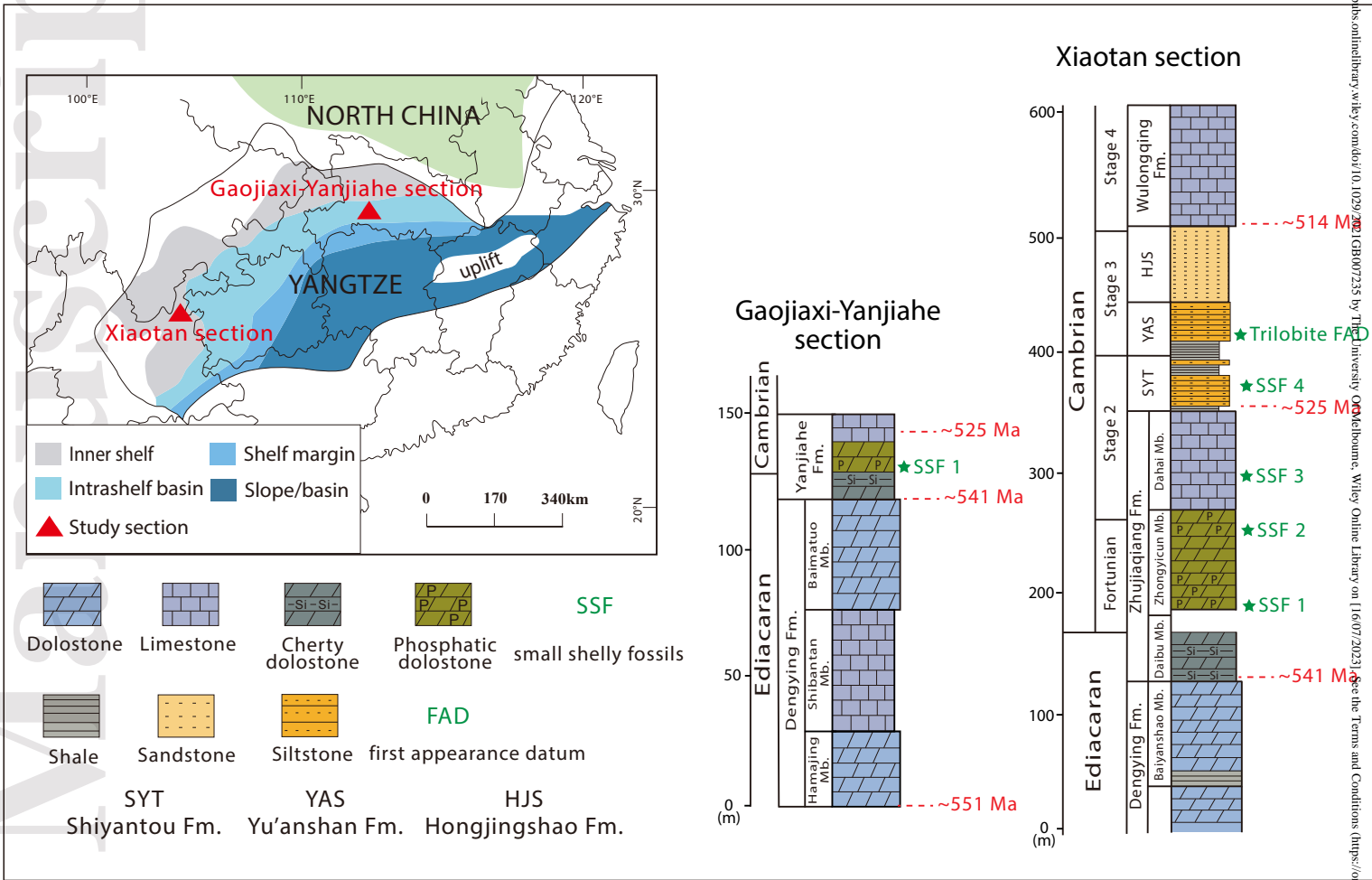
Figure 2. Thin sections from the studied carbonate samples under a polarizing light microscope. (A) micrite or microsparite in the Dahai Mb., Xiaotan section; (B) dolomicrite interbedded with phosphorite in the Zhongyicun Mb., Xiaotan section; (C) coarsely crystalline cherty dolostone in the Daibu Mb., Xiaotan section; (D) dolosparite or dolomicroparite in the Dengying Fm., Xiaotan section; (E) dolomicroparite in the lower Yanjiahe Fm., Gaojiaxi–Yanjiahe section; (F) dolomicrite in the Dengying Fm. (Baimatuo Mb.), Gaojiaxi–Yanjiahe section.

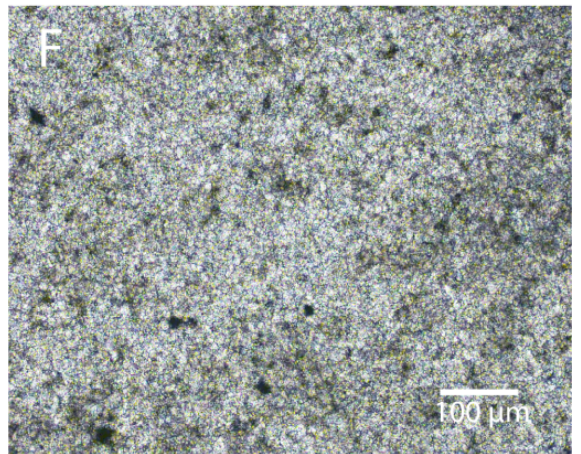
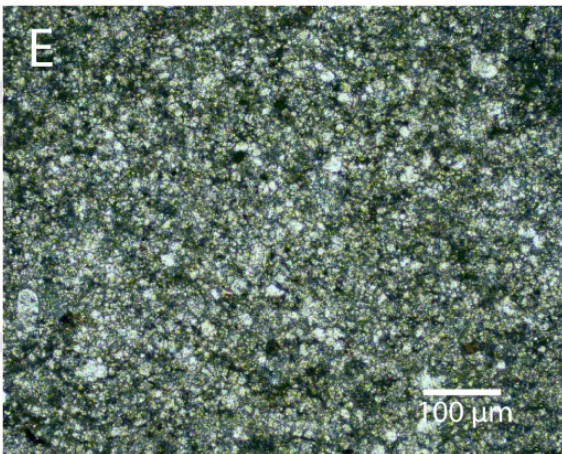
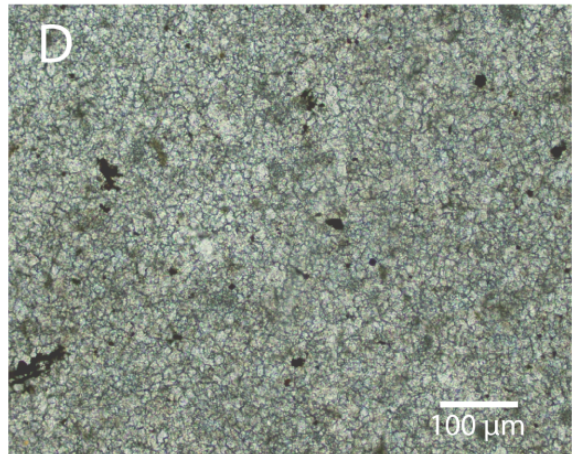
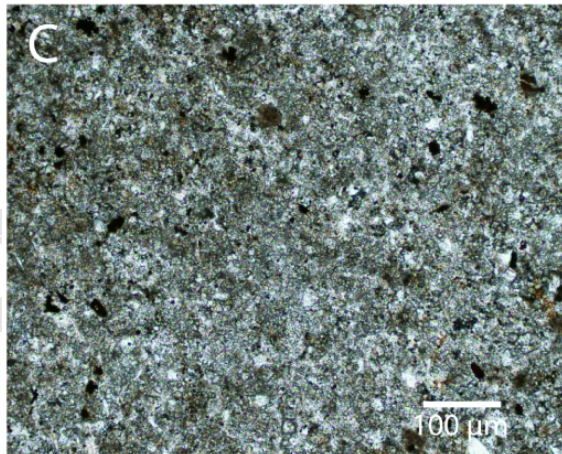
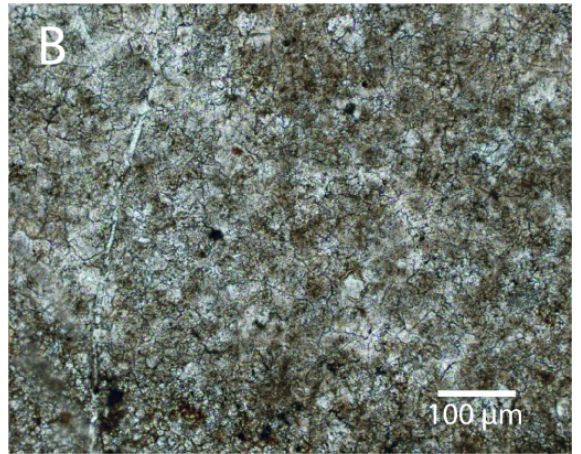
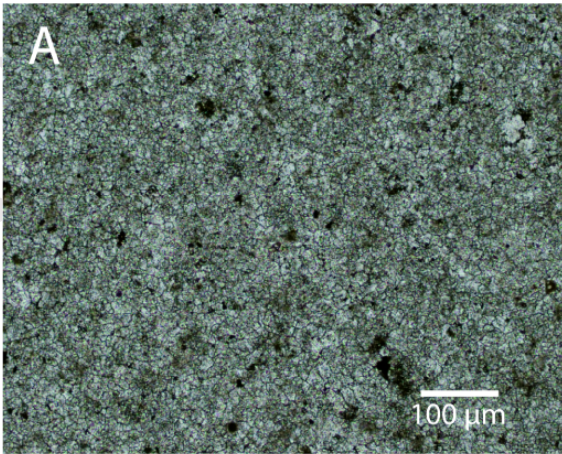
Figure 3. Geochemical profiles of the Gaojiaxi–Yanjiahe section and the Xiaotan section. The dashed lines represent average $\delta^{44}\text{Ca}$ values and Sr concentrations of modern Bahamian aragonites and calcites (Higgins et al., 2018).

Figure 4. Compilations of Ca isotope and Sr concentration data from the upper Ediacaran to lower Cambrian sections analyzed for this study. (A)–(D): Distributions of $\delta^{44}\text{Ca}$ values for the upper Ediacaran to lower Cambrian carbonates in this study. (E) and (F): temporal changes in $\delta^{44}\text{Ca}$ and Sr contents of the studied carbonates. Black dashed lines denote average $\delta^{44}\text{Ca}$ values of modern Bahamian carbonates (Higgins et al., 2018).

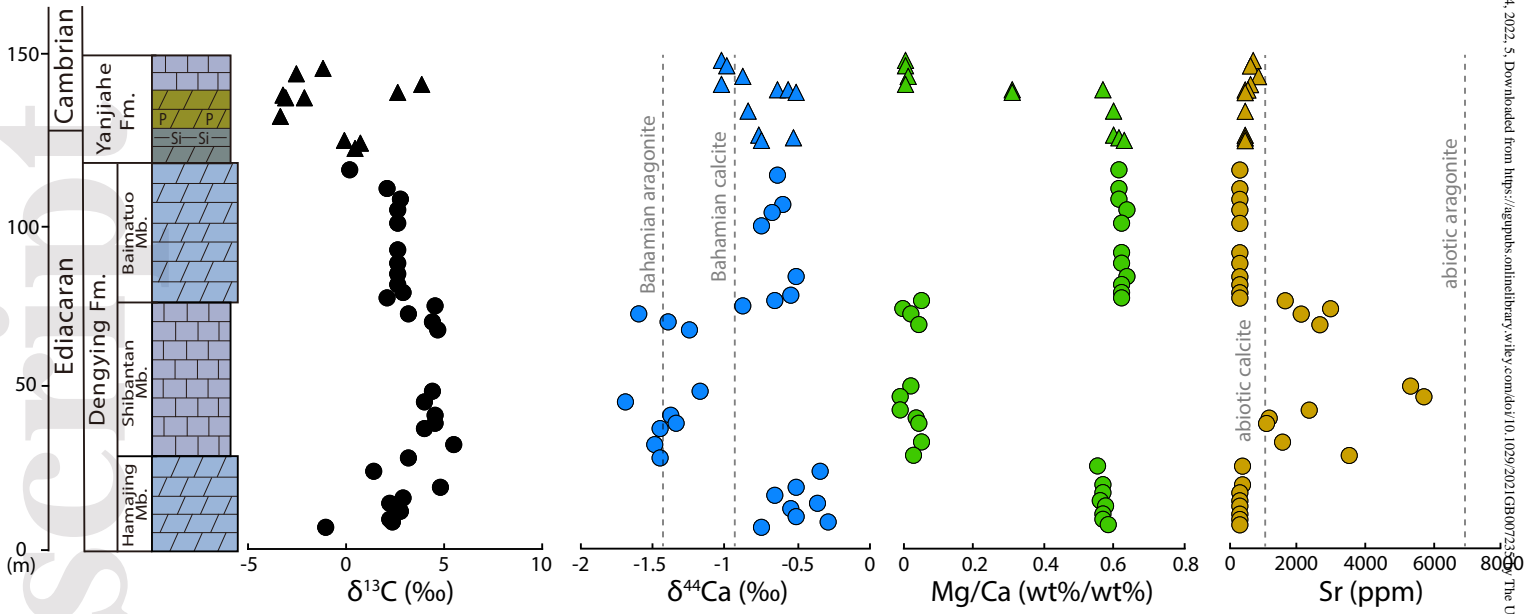
Figure 5. Cross-plots of $\delta^{44}\text{Ca}$ vs. Mg/Ca ratio (A) and Sr content (B and C) for the studied carbonates in South China as well as limestones from the Nama Group, Namibia (Tostevin et al., 2019), and results of application of a shallow-marine diagenetic model (Ahm et al., 2018). In (B), the solid lines represent pathways for marine dolomitization of primary aragonite, whereas the dashed lines represent neomorphism from primary aragonite to the present calcite. In (C), the solid lines represent potential pathways of marine dolomitization of primary calcite, whereas the dashed lines represent recrystallization of primary calcite. Black arrows in each figure panel represent the extent of alteration of the bulk sediment (from 0% to 100%, following the direction of arrow) under different pathways of diageneses. Blue lines represent the range of compositional variability circumscribed by a fully diagenetic mineral derived from a fluid-buffered endmember to a sediment-buffered endmember. The purple solid lines in (C) denote rate-controlled correlations of $\delta^{44}\text{Ca}$ values and Sr contents under different seawater conditions (Tang et al., 2008; Wang et al., 2020 and references therein).

Figure 6. Compilations of geochemical and petrographic data in non-skeletal carbonates from the late Ediacaran to the Cambrian. (A)–(B) Geochemical compilations include both the Ca isotope and Sr/Ca data produced in this study and previously published data. Whiskers denote the minimum and maximum of data within 1.5 times the interquartile range from the median. Blue boxes represent data generated from limestone samples and orange boxes represent those generated from dolostone samples (see Supplementary Table S2 for data sources). (C) Petrographic compilations denote the distribution of different minerals (dolomite, aragonite, high-Mg calcite, low-Mg calcite) in non-skeletal carbonate phases (i.e., cements and ooids) from the upper Ediacaran to the Cambrian (see Supplementary Table S1). (D) Estimations of global anoxic seafloor area (red curve, based on U isotope data) (Wei et al., 2021a), atmospheric oxygen level (black curve, based on GEOCARBSULFOR model; Krause et al., 2018), and atmospheric/oceanic oxygenation level (gray area, based on Fe speciation data; Sperling et al., 2015).





A. Gaojiaxi-Yanjiache section



B. Xiaotan section

